The Pennsylvania State University
The Graduate School
College of Engineering

COMBINED STATE OF CHARGE AND STATE OF HEALTH ESTIMATION FOR LITHIUM-ION BATTERIES

A Thesis in
Mechanical Engineering
by
Aabhas Sharma

© 2012 Aabhas Sharma

Submitted in Partial Fulfillment
of the Requirements
for the Degree of

Master of Science

August 2012

The thesis of Aabhas Sharma was reviewed and approved* by the following:

Hosam K. Fathy
Assistant Professor of Mechanical Engineering
Thesis Advisor

Christopher D. Rahn
Professor of Mechanical Engineering

Karen A. Thole
Professor of Mechanical Engineering
Department Head of Mechanical and Nuclear Engineering

*Signatures are on file in the Graduate School.

Abstract

This thesis examines the challenges faced in combined State of Charge(SoC) - State of Health(SoH) estimation for lithium ion (Li-ion) batteries. To monitor battery state (both long term and short term), it is imperative to analyze the factors affecting the errors in estimation of SoC and health parameters such as capacity and internal resistance. A brief survey of the literature is done for the state-of-the-art in battery state estimation and control with respect to the above stated parameters. Estimation of SoC, capacity and resistance over an extended period of use is studied using a first order equivalent circuit model to demonstrate the fundamental challenges faced in simultaneous estimation. Identifiability of system parameters pertaining to persistence of excitation (PE) in input signal and flatness of open circuit voltage(OCV) vs. SoC curve is studied using an Extended Kalman Filter,least squares estimation algorithm and Cramér-Rao bounds. Mathematical derivations supported by simulation studies are done to observe the effect of individual factors including noise levels, PE dither, SoC ranges, time and initial conditions on estimation error. A trade-off discussion supported by Monte-Carlo simulations is finally presented to explain the influence and importance of each factor pertinent to SoC-SoH diagnostics, prognostics and control.The results suggest that battery SoC-SoH parameter identifiability is dependent on: (1) Higher regions of the OCV-SoC curve which give better capacity estimates (2) PE dither which helps gain accuracy in resistance estimation.

Table of Contents

List of Figures

List of Tables

Acknowledgments

I would like to take this opportunity to acknowledge everyone who has helped me made this thesis possible.

I would like to express my sincere gratitude to my advisor, Dr. Hosam Fathy, whose constant guidance, advice and mentoring has made not only this research possible but also had helped me grow as an individual both academically and socially. I would also like to thank Dr. Christopher D. Rahn for being an invaluable member of my committee and his deep insights which have molded this thesis into its present form.

I would like to thank everyone in the Control Optimization Lab (at The Pennsylvania State University and The University of Michigan) for their encouraging and constructive feedback on my work. I owe a great debt to Dr Saeid Bashash, who in Hosam's words was my 'real mentor'. His immense knowledge, combined with his modesty and his willingness to help me with both labwork and framing my thesis has been extremely instrumental. I want to thank Scott Moura, Joel Forman and Rakesh Patil for their incredible help with regards to experimental work. Thanks to Kelsey Hatzell for her insights and discussions on our research, and to Michael Rothenberger, Michael Beeney, Sergio Mendoza and Tim Montgomery for their honest and extremely helpful feedback which has made me continuously improve my work.

Most importantly, I would like to thank my parents, Rashmi and Raj Kumar Sharma and my younger sister, Aakrati, for being my pillars of strength and support at all times and at all distances. Thank you for forever encouraging me and continuously inspiring me as role models. This thesis would not have been possible without you.

Finally, I would like to thank my roommates(present and former), friends and family in the US, State College and India for their constant support and help that has made this journey all the more enjoyable.

Chapter 1

Introduction

1.1 Overview

This chapter provides a brief introduction to the importance of Li-ion battery state estimation, its role in the energy sector and the need for designing better algorithms to monitor short-term and long term battery health.

1.2 Introduction

Batteries have emerged as an important part of the solution to the energy crunch[1]. They provide one of the higher energy density options available when choosing an alternative energy source for applications such as electric vehicles (EVs), hybrid electric vehicles (HEVs), plug-in hybrid electric vehicles (PHEVs), grid storage and portable electronics. A Ragone plot compares the power and energy capabilities of different energy storage systems. Various energy conversion systems are shown to demonstrate their specific energy capabilities in Figure 1.1. An example of a vehicle powered by different energy conversion systems including a gasoline powered engine shows that in comparison to various battery chemistries, lithium-ion systems have a greater driving range per kilometer for the same battery wight and fuel tank size[1]. Characteristics such as high cell voltage, low memory effect, low self-discharge rate (compared to nickel batteries) and higher energy density have led to an increased interest in the design of better chemistries and algorithms for control applications[2].

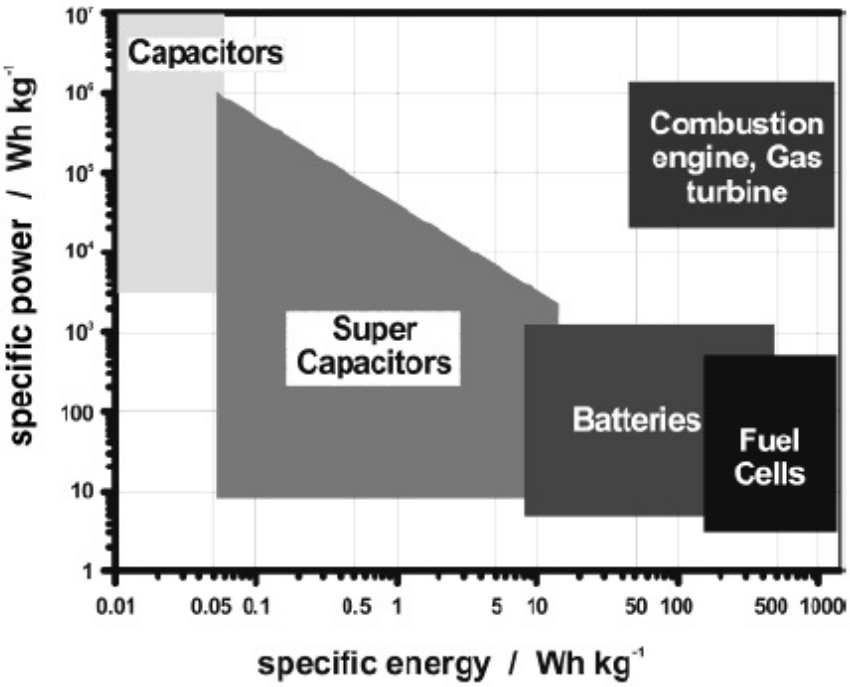

Figure 1.1. Simple Ragone plot comparing different energy storage systems, obtained from [1]

Studies relating to Li-ion battery sizing, design, and control for various applications, thus become important in order to get benefits such as longer range or extended life. It is important to analyze battery lifecycle costs, for which the study of battery degradation through continuous use, over a period of time becomes important. The need to replace a battery plays an important role in the lifecycle cost and studies related to this are discussed in[3].

Three main reasons motivate the research in this thesis. First, there is a need to develop an accurate estimator for battery SoC, capacity and resistance to know the state of a battery in terms of its capability to provide charge, its overall capacity and loss of power. From an industrial level, it is important to know the current condition of the battery for replacement, repair and longevity purposes. From a research perspective it helps develop better control strategies, optimal charge-discharge patterns and improved materials for long term usage. Second, there is a need to examine some factors that affect the accuracy of such an estimator, namely persistent excitation of input, flatness of OCV-SoC curve and identifiability of sim-

ple equivalent circuit models in relation to estimation. Finally, there is a need to study the inter-dependence of these factors and their effect on the estimation of the names parameters (SoC, resistance and capacity). Battery SoC, at a given temperature, is defined as the ratio between the actual amount of charge in a battery to the total amount of usable charge at a given charge/discharge rate[4]. Battery SoH has been defined in multiple ways which will be explained in detail in Chapter 2. SoC and SoH differ from each other in the way they affect the battery chemistry, where SoC is a measure of charge available over a single charge/discharge cycle and the changes occurring in a battery are reversible. SoH refers to the reduction in capacity or increase in internal resistance due to the irreversible changes occurring in a battery over prolonged use. They also differ in the rate at which they occur with SoC being a measure for short term (hours and days)and SoH being a measure for longer period of continuous use (months and years). Capacity fade and power fade are the two phenomena associated with battery SoH. Loss in overall capacity of the battery due to continuous use over a period of time is known as capacity fade. Power fade is the increase in internal impedance, which in turn reduces the amount of power available from the same battery.

The remainder of the thesis is organized as follows : Chapter 2 briefly reviews the current advancements in battery SoC and SoH literature, the challenges and need for better estimation algorithms. Chapter 3 goes over the problem formulation for the work, using a simple equivalent circuit model for describing the issues with techniques used. The simulations for proposed solutions to the challenges are described in Chapter 4 which also delves into fundamental trade-offs for the better design of an estimation algorithm. In Chapter 5, we conclude with a brief overview of the problem tackled in the thesis and its potential in possible future work.

Chapter 2

Literature Review

2.1 Introduction

This section provides a brief introduction to the battery State of Charge(SoC) and State of Health(SoH) estimation literature. To control Li-ion battery (LIB) charging and discharging in a health conscious manner, one needs to estimate battery State of Charge (SoC) and State of Health (SoH) online. This section reviews the techniques employed for battery SoC and SoH estimation focusing on different applications where online estimation and error limits are factors influencing the design of estimators. Aggressive battery use increases the need for SoC/SoH estimation to ensure efficiency, avoid overcharge/overdischarge, and facilitate condition-based maintenance[5]. We begin with a brief discussion of SoC estimation, then focus on the relatively less-explored SoH estimation problem. Finally we conclude the chapter by identifying potential challenges in parameter identifiability in combined SoC-SoH estimation, which serve as motivators for this thesis.

2.2 State of Charge (SoC) Estimation

State of Charge estimation is a relatively well-explored research problem. Much of the SoC estimation literature explores the use of linear equivalent circuit models in conjunction with either open-loop estimation methods (e.g., Coulomb counting) or closed-loop methods (e.g., Kalman Filtering) to determine the state of charge from input current and terminal voltage measurements[6].

The challenge of online estimation is tackled by Plett in a series of papers that describe the process of modeling the battery as an equivalent circuit (with different charge/discharge resistances) with SoC estimated as a state variable and a term for hysteresis in the output equation[7, 8, 9]. An extended Kalman Filter is applied to these models to estimate SoC with dynamic error bounds on the estimate. Coulomb counting has emerged as one of the most commonly used techniques for SoC estimation[10, 11]. Ng *et al.* propose an enhanced estimation method based on coulomb counting. Based on current and voltage measurements the battery state is determined to be in either charge, discharge or open-circuit stage and SOC relations are established for each. These relations are then used to estimate SoC over a cycle, resetting different parameter values at the start of every estimation. This method is highly dependent on knowing exactly which state the battery is in and also the time of examination. Open-loop estimation via coulomb counting is subject to errors due to measurement so model based algorithms require a good cell model. Codeca *et al.* present a 'mixed' solution which incorporates coulomb counting along-with model-based estimation for SoC [12]. An algorithm combining both, where the coulomb counting captures the fast dynamics as the feed forward component of estimation and model based approach corrects the estimate in a closed loop control system. Estimators that capitalize on fundamental nonlinearities in battery dynamics and are robust to uncertainties for online applications use other methods such as fuzzy logic and autoregressive moving average models for prediction[13, **?**]. The need for historical data, training and high instrument cost such as electrochemical impedance spectroscopy limit the use of these methods in real time applications.

The challenge associated with electrified vehicle applications is the fact that the large battery currents seen in such applications tend to excite complex dynamics that equivalent circuit models typically do not capture (e.g., finite and infinite-dimensional diffusion dynamics, etc.). This has motivated research in the development of electrochemistry based battery models. The use of reduced order models for SoC estimation has been experimentally verified for low C-rates and measured drive cycles of hybrid vehicles. Chaturvedi *et al.* determine the volume averaged concentration of each electrode through a linear corrective observer with output injection[14]. The results obtained are compared against commercial

18650 Li-ion cells to show that the observer is able to estimate SoC based on the definition in Equation 2.1,

$$SOC^{-} = \frac{1}{L^{-}} \int_{0^{-}}^{L^{-}} \frac{\overline{c}_s^{-}(x,t)}{c_{s,max}^{-}} dx \tag{2.1}$$

where the negative sign signifies negative electrode. The observer is also able to estimate voltage in the presence of measurement noise and initial bias. A 1-D spatial first-principles based model that assumes a single particle for each of the electrodes in the battery is developed and used for voltage and SoC estimation. The electrolytic movement is modeled using macroscopic properties in a single direction whereas the diffusion dynamics are modeled microscopically within the spherical particle[15, 16, 17, 18]. The models thus created are used to predict the average concentration profiles at both the electrodes and then SoC as a non-dimensional quantity using the maximum and predicted concentrations. Maintaining constant cell temperature is important for accurate estimates and parameters show a temperature dependency. Stefanopolou *et al.* implement an extended Kalman Filter with output nonlinearity to show that the concentration profile can be estimated correctly from an initial error. The approach is able to incorporate nonlinear dynamics of the battery but starts developing errors in estimation for large values of currents or relaxation after a current pulse. Santhanagopalan *et al.*.also use an extended Kalman Filter for online SoC estimation using two case studies based on process and measurement noise. Each case studies the effects of the noises individually on the prediction of SoC and the conclusions are verified against experimental data. K.A. Smith *et al.* reduce a full Doyle Fuller Newman [19] battery model into a 1-D model for control applications. Analytically derived transfer functions and numerical transfer matrices are derived to describe output response in relation to an input current with solid and electrolyte concentrations as variables [20]. These are done assuming linearity of battery properties and decoupled reaction current from electrolyte concentration. This study is compared and contrasted to another reduced model by Speltino *et al.* in [21].

Thus, increasing the complexity of the battery model helps in better estimation but the equivalent circuit model is able to capture key dynamics accurately and can be used as a tool for SoC estimation studies. It enables us to simulate the

battery under real time conditions to study the effects of parameters such as measurement noise, input excitation and OCV-SoC slope. The observability, stability and identifiability issues faced when the SoC estimation is combined with SoH estimation using a simple equivalent circuit model are not discussed extensively in the literature. This serves as a motivation to the research done in this thesis. The next section looks at the literature of SoH estimation either in terms of OCV, capacity, resistance or a combination of them.

2.3 State of Health(SoH) Estimation

Compared to SoC estimation, the equally important battery health estimation problem remains relatively unexplored. Typically, over a period of use, the battery undergoes many irreversible changes that have to be accounted for in order to determine the battery's state on a daily basis. These factors including but are not limited to, Solid Electrolyte Interphase (SEI) layer growth, dendrite formation, lithium plating, thermal aging and mechanical degradation leading to degradation and eventual death[22, 23, 24] . Capacity fade and power fade have become the primary areas of study and parameters related to them, namely capacity and resistance of the battery, are estimated.

Several physics based battery models have been analyzed to study battery degradation and use them for prediction purposes. Ramadass *et al.* analyze capacity fade in Li-ion batteries by building a semi-empirical mathematical model using experimental data to capture the variation in parameter related to capacity fade using two approaches[25]. The two approaches model the total capacity fade as a result of increase in film resistance active material loss and rate capability loss. SoC is attributed to account for active material loss and the diffusion coefficient of the limiting electrode accounts for rate capability losses. According to the authors, the predictive model is successful in providing better accuracy but the problem of specificity of the correlations to a particular battery chemistry and geometry serve as limiting factors. The effect of temperature and cycling on capacity fade is used to construct an analytical model for remaining battery capacity prediction is also explored by Rong *et al.* in [26]. Online estimation algorithms with current and voltage measurements are verified against actual life-cycle data.

Aggregates of realistic drive cycles from the Urban Dynamometer Driving Schedule and driving survey data are used to create a driving profile to study cell degradation related to depth of discharge (DOD) and discharge rates[27]. The effect of higher rates being more important than DOD is reinstated. Saha *et al.*use experimental battery testing data to construct predictive aging models that serve as the 'plant models' within a battery prognostics and diagnostics algorithm[28]. An equivalent circuit model with exponential degradation dynamics is created and parameter identification is done through particle filtering using relevance vector machines. Capacity fade is also analyzed using a matrix of experiments to include five different temperatures, depth of discharge levels and discharge rates[29]. While time and temperature become major factors at low rates, a power law is created at higher rates to include the rate effects with time. The multiplicity of different SoH estimators in the literature tackle problems as disparate as estimation of the charge capacity of a battery using open-loop Coulomb counting versus estimating internal resistance and open-circuit voltage versus amount of charge stored in a given battery cell for different levels of aging[30].

The equivalent circuit model has been used commonly to build estimators for SoH prediction. Various estimation algorithms to get closer accuracy, improve convergence and enhance speed are used for capacity and resistance prediction. Chiang *et al.* formulate an adaptive algorithm around an equivalent circuit model to estimate OCV and internal resistance as parameters[31]. Authors highlight the importance of persistent excitation (PE) of the input signal through measurements related to the driving pattern. Capacitance of the circuit (representative of battery capacity) is not evaluated owing to this but OCV is estimated online within 1% relevant SoC error after internal resistance estimation is done accurately. V. Pop *et al.* examine the errors in SoC estimation and its effects on determining capacity (remaining run time)[32]. The paper defines various states of battery operation including initial, standby, charge, discharge and transitional, establishing relationships and determining sources of error for each. Remaining run time is calculated based on SoC estimation which is dependent on the accuracy of the model. Algorithms that track changes in capacity over every cycle are shown in Tang *et al*[33]. The auhors use least squares estimation to predict SoC and capacity for batteries in plug-in hybrid electric vehicles (PHEVs) using a second order equivalent circuit

model. The paper explores two different modes : driving and plug-in charge, citing the lack of excitation in the latter mode. Due to this, lookup table for SoC is preferred and current integration is used to calculate capacity. In the former, for every operative cycle the capacity estimate is obtained through a multiplication of OCV-SOC slope (from a lookup table obtained via experiments) and a paramater keeping track of current integration. Convergence speed is determined by excitation levels in the driving profile. Verbrugge *et al.* implement a weighted recursive least squares estimator for OCV and resistance estimation[34]. Forgetting factor for setting the weight of the estimator is examined, where a smaller values is desirable for estimating OCV and a large value for resistance. Also, varying the forgetting factor improves accuracy of the algorithm. Rapid improvements in automotive battery materials are furnishing new LIBs with both reduced self-discharge and flatter characteristic curves relating open-circuit potential to state of charge. One negative consequence of these improvements is the fact that state of charge is less observable/detectable for these newer batteries compared to their predecessors. A solution to this problem is proposed in [35, 36]. An equivalent circuit model with parameters established through time domain analysis and voltage source as function of SoC is considered. A dual extended Kalman Filter for SoC and capacity estimation is applied to the model with a measurement noise model which varies the measurement noise based on the current input, voltage error and SoC values and data rejection technique applied to compensate for errors caused due to fast dynamics.

2.4 Challenges identified from literature

From the above literature, we are able to observe some specific challenges in identifiability of parameters for combined SoC-SoH estimation. Battery aging dynamics are complex, intertwined and have similar time constants making it difficult for the progress of battery aging effects to be estimated online based on voltage and current measurements. The close interrelation of SoC, capacity and resistance, even in the simplest of equivalent circuit models, makes the simultaneous estimation problem challenging as the change in one parameter directly influences the observability of others. The time separation in the dynamics of SoC and SoH parameters

should also be considered in the estimation algorithm. Inherent lack in excitation for testing, flatness of the OCV-SoC curves in the new chemistries for reliable operation, and sensor noise levels are some key issues in the development of better health estimators. Thus two main challenges for identifiability of parameters in combined SoC-SoH estimation are :

- Lack of persistent excitation (PE) in the CC and CV parts of the CCCV charge-discharge cycle
- Flatness of the OCV-SoC curve influencing the capacity estimate

This, in turn, makes it very challenging to estimate the health of LIBs online, predict their death, and control them in a manner that postpones such death, which motivates the research in this thesis. The exploration of battery state identifiability (SoC and SoH), factors influencing estimation (excitation in input, OCV-SoC curve) and challenges with sensors (voltage and current) remains an open area of research which can provide a better mean for onboard battery health prognostics, diagnostics and control.

The next chapter looks at the mathematical analysis done to describe the challenges associated with combined SoC-SoH estimation in terms of the system's parameter identifiability, with respect to persistence of excitation and OCV-SoC curve flatness.

Chapter 3

Mathematical Analysis

3.1 Introduction

In the previous chapter, the state-of-the-art battery SOC and SOH estimation was discussed. This thesis looks at an equivalent circuit model for combined SoC-SoH estimation. A Li-ion battery is a complex electrochemical system which has been modeled in several ways, each varying in the degree of complexity. An equivalent circuit is the simplest model representing the battery's dynamics. The literature surveyed in the previous chapter described how the equivalent circuit model is able to capture the systems dynamics of a battery. It is important for describing our problem, since if the problem can be discussed via simplistic assumptions then the literature needs to look into these before increasing complexity of models or algorithms. Also, this chapter will discuss some of the basic areas that are often overlooked in the design of estimators for health prognosis. The problem that we tackle in this thesis is defined in section 3.2. In section 3.3 the characteristics of the equivalent circuit model and equations related to it are discussed. The experiment conducted to obtain the OCV-SoC curve and sensor noise values is discussed in this section. The observability problem for an Extended Kalman Filter is discussed in section 3.4. Sections 3.5 and 3.6 discuss a simple least squares estimation algorithm and implementation of the algorithm for our equivalent circuit model. Two issues/challenges that were identified from the literature were the persistence of excitation of the input signal (in a CCCV cycle) and the flatness of the OCV-SoC curve. These are illustrated via mathematical derivations in sections

3.7 and 3.8 respectively. The Cramér-Rao bounds are derived for our estimator to show how the estimated parameters are dependent on sensor noise, slope of the OCV-SoC curve and input current. The chapter ends with a prelude to the simulations done to illustrate the challenges.

3.2 Problem Definition

This thesis intends to explore the challenges faced during SoC-SoH estimation. An observer can be constructed to estimate SoC and SoH individually and simultaneously, as was discussed in the previous chapter. The goal is to design an estimator for battery state of charge, capacity and internal resistance simultaneously given input-output data (current and voltage).

3.2.1 Subproblems

For all online applications, sensor noise is present in the measurements made for estimation. In our model, current and voltage sensors have to be used for obtaining measurements and these values are noisy. The noise variances were obtained as explained in the previous section. The degree of noise is important for determining how accurate the estimator would be. This is explored via simulations in the next chapter.

This thesis attempts to estimate SoC, capacity and ressistance using a single simulation. Since the state and parameters are interrelated through the mathematical relations described earlier, this is not a trivial problem and often the estimates fail to converge. Thus it becomes important to limit the divergence of the estimates within certain range. For this thesis, we have limited the divergence of the parameter estimates to within 50-150% of the initial approximation. If their values diverge below or above the setpoints, then the values are set to the initial approximation.

The estimator system stability and observability of the model are issues that are encountered during the analysis. The observability of the system is dependent on the linearization point and the nominal value of input. Hence it becomes important to explore the conditions under which the system is observable. This will be

explained in further detail in Section 3.4.

Constant Current Constant Voltage (CCCV) is a generic charge-discharge process used to analyze the behavior of Li-ion batteries. During charging, the battery is subjected to a constant current which leads to a rise in the voltage of the battery [37]. When the battery hits a threshold upper voltage, it is allowed to stay at that voltage for constant voltage charging. During this period the relaxation occurs and the battery is further filled to its utmost capacity. This also causes a drop in the current. Once the current drops to a lower threshold value, the battery is said to be fully charged and can be used for charge extraction. For a system to be identifiable, it is necessary that it should be persistently excited. Inherently, the CC and CV parts of the CCCV cycle process are not individually persistently exciting and this creates an identifiability problem for the parameters. This problem is explained in detail in Section 3.7.

The OCV-SOC curve has been shown earlier in the thesis as being an important factor for relating the output voltage to SoC. As can be seen, there exists a flat region from 20-80% SoC where the change in voltage is very small for a prolonged change in SoC. Thus, the SoC estimation problem becomes difficult because for a given voltage value the SoC could be as high as 70% or as low as 30%. Also, for the implementation of an observer, linearization is used and the slope at every given point of time should be accurately known for estimating the other parameters. This challenge is also discussed in detail in Section 3.8 .

Considering all the above stated challenges in SoC-SoH prediction, the intent is to study them and come up with possible solutions to understand the shortcomings for estimation and aid the construction of a robust estimator. We conclude that the observability/identifiability of the system's parameters is a challenge owing to :

1. Persistence Excitation of input signal
2. Flatness of OCV-SoC curve

We examine the problem using three different approaches :

1. Extended Kalman Filter
2. Least Squares Estimation

3. Cramér-Rao bounds

Although all three are different methods, we will see that we can arrive at consistent conclusions from each.

3.3 Equivalent Circuit Model

The equivalent circuit model is the simplest model representing a Li-ion battery. The dynamics of the battery are captured to a level of accuracy which can be used for online applications and validation purposes. For our purpose, we have represented the open-circuit voltage by a voltage source. This open-circuit voltage is related to the SoC through a OCV-SOC curve. A resistance is modeled in series to capture the internal resistance of the battery. A pictorial representation of this model is shown in Figure 3.1. State of Charge, capacity and resistance are the states in the model, with input as current and output as voltage. The health parameters of the battery, namely resistance and capacity, are assumed to be constant over the time period of simulation.

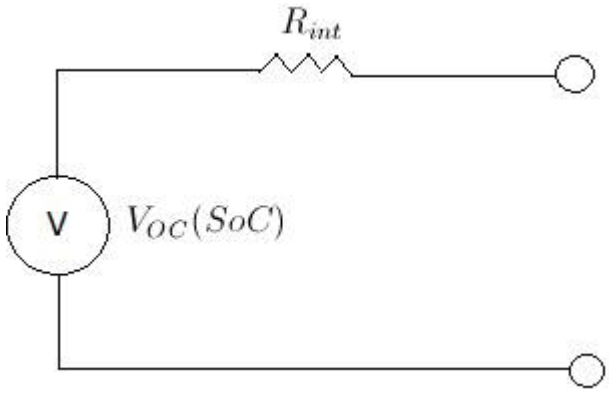

Figure 3.1. Equivalent Circuit Model

We can thus obtain a equations representing our battery as :

$$\dot{SoC} = \frac{I}{Q} \tag{3.1}$$

$$\dot{Q} \approx 0 \tag{3.2}$$

$$\dot{R} \approx 0 \tag{3.3}$$

$$V = V_{OC}(SoC) + IR \tag{3.4}$$

Equations 3.1-3.3 are the state equations of the model. Variation of capacity and internal resistance with time is orders of magnitude slower than the simulation time for our estimation and hence they are assumed to be constant. Current being drawn or being supplied to the battery is the input. The final equation is the output equation which is obtained by circuit analysis.

3.3.1 Obtaining the OCV-SoC Curve

The OCV-SOC curve is important for simulating the model. A slow charge-discharge test is performed to obtain the curves. For our purpose, an A123 26650 $LiFePO_4$ battery, with a capacity of 2.3 A-h was subjected to a 0.1C charge and discharge. The upper and lower bounds on the voltage for the test were 3.8V and 2.2V respectively. The voltage limits define our charge and discharge limits. A battery is declared to be at 100% SoC (fully charged) when the voltage hits 3.8V and 0% SoC (fully discharged)when the voltage reaches 2.2V. All of the measurements were done at room temperature (25^oC). The curve obtained through the test is shown in Figure 3.2.

The separation between the charge and discharge curves is due to polarization effects in the battery. We take the average value and perform our simulations for the average curve. A 5th and 10th order polynomial were then fitted to the curve using MATLAB®'s *polyfit* command. The fits obtained are shown in Figure 3.3. Figure 3.4 shows the error in voltage due to the fitting. The 10th order polynomial seems to fit the OCV-SoC curve accurately and hence we use it for our simulation. The 10th order polynomial is listed in Equation 3.5 which is used from now onwards as the OCV-SOC relation in the rest of the document.

$$\begin{aligned} V_{OC}(SoC) = {} & 29.02 * SoC^{10} + 3103 * SoC^9 - 14500 * SoC^8 \\ & +28300 * SoC^7 - 30400.0 * SoC^6 + 19700.0 * SoC^5 \\ & -7903.0 * SoC^4 + 1942.0 * SoC^3 - 279.3 * SoC^2 + \end{aligned}$$

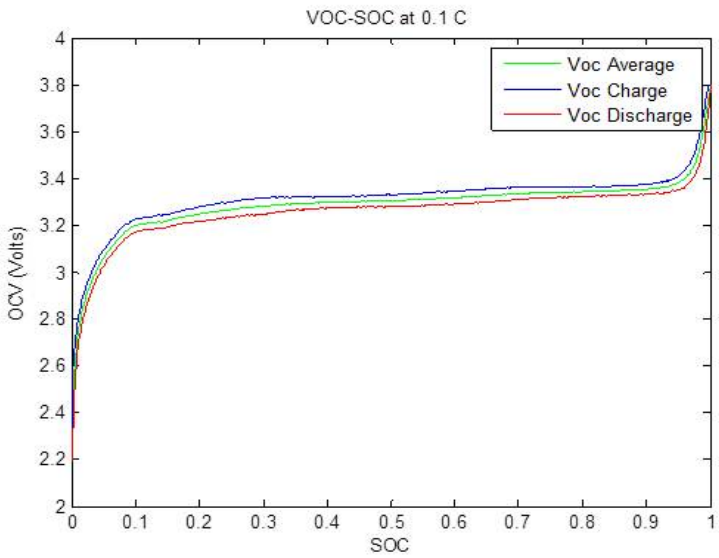

Figure 3.2. OCV-SoC Curve obtained for 0.1C Charge-Discharge

$$21.78 * SoC + 2.488$$

From the experiments done to obtain the OCV-SoC curve we can obtain the distribution of the sensor noise values. In order to obtain the noise distribution, we constantly measure the current and voltage values during the experiment. During the CC part, the actual value of current is subtracted from the measurement values of current to obtain the noise of the sensor and a histogram is plotted to show the frequency of occurrence. A similar process is repeated during the CV part to get the voltage sensor noise distribution. These distributions are shown in Figure 3.5. These noise values are assumed to follow a Gaussian distribution with zero mean and the standard deviations can thus be calculated.

The standard deviation of the current and voltage sensor noise were obtained as :

$$\sigma_I = 10mA, \qquad \sigma_V = 1.5mV \tag{3.5}$$

Now that all the mathematical relations are established the next step is to explain the possible challenges in estimating SoC-SoH using fundamental math-

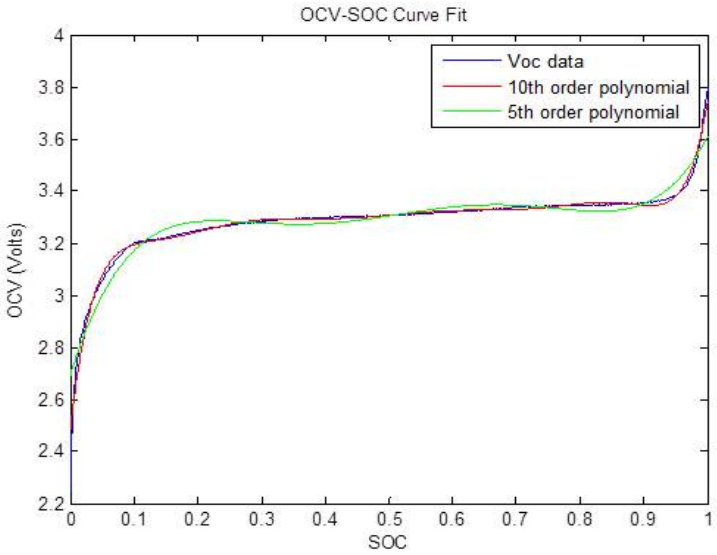

Figure 3.3. 5th and 10th Order Polynomial Fits to OCV-SoC curve

ematical derivations. Deductions are made at the end of each section which are then looked at via simulations in the next chapter.

3.4 Observability using Extended Kalman Filter

The model explained earlier in the thesis should be observable for an estimator to be built around it. We initially decided to use the Extended Kalman Filter theory to study the observability conditions for our model. Thus, to check observability we obtain a linearized state space model of the system, under the assumption that resistance a known parameter but SoC and capacity (Q) are the states to be estimated. Hence our system now becomes:

$$\dot{SoC} = \frac{I}{Q} \tag{3.6}$$

$$\dot{Q} \approx 0 \tag{3.7}$$

$$V = V_{OC}(SoC) + IR \tag{3.8}$$

Now we get the state space representation as

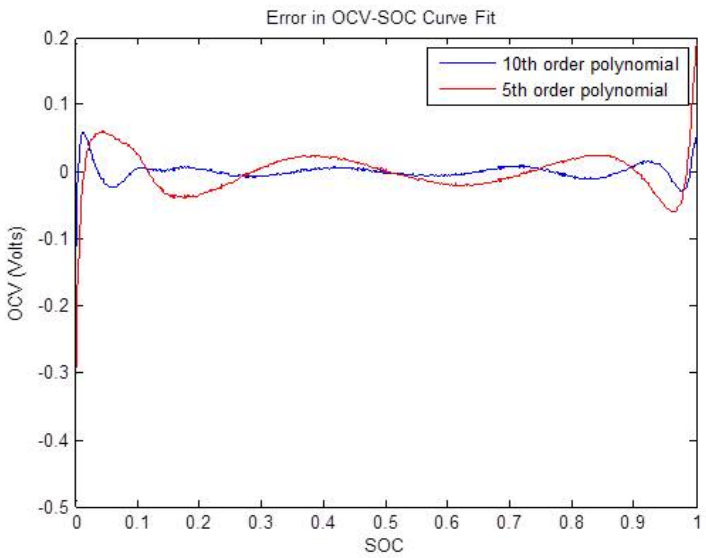

Figure 3.4. Error in 5th and 10th Order Polynomial Fits to OCV-SoC curve

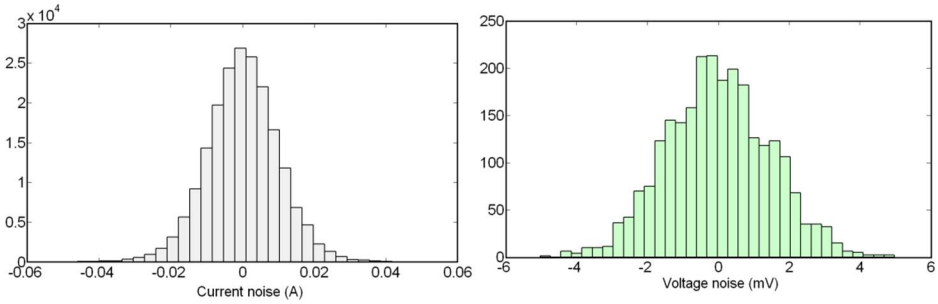

Figure 3.5. Histogram of Current and Voltage Noise Distribution

$$\dot{x} = \begin{bmatrix} 0 & -\frac{I_0}{Q_0^2} \\ 0 & 0 \end{bmatrix} x + \begin{bmatrix} \frac{1}{Q_0} \\ 0 \end{bmatrix} u \tag{3.9}$$

$$y = \begin{bmatrix} \frac{\partial V_{OC}}{\partial SoC} & 0 \end{bmatrix} x + \begin{bmatrix} R_0 \end{bmatrix} u \tag{3.10}$$

Here I_0 is the nominal current, Q_0 is the nominal capacity, R_0 is the nominal internal resistance, u is the input, y is the output and x is the state vector. Now we will look at how the observability is affected by these values.

The observability matrix is defined as

$$O = \begin{bmatrix} C \\ CA \end{bmatrix} \tag{3.11}$$

For a system to be observable the observability matrix should be full rank. Our system has the following A and C matrices, to give the observability matrix

$$\begin{aligned} A &= \begin{bmatrix} 0 & -\frac{I_0}{Q_0^2} \\ 0 & 0 \end{bmatrix} \\ C &= \begin{bmatrix} \frac{\partial V_{OC}}{\partial SoC} & 0 \end{bmatrix} \end{aligned} \tag{3.12}$$

So we get O, which is the observability matrix,

$$O = \begin{bmatrix} C \\ CA \end{bmatrix} = \begin{bmatrix} \frac{\partial V_{OC}}{\partial SoC} & 0 \\ 0 & -\frac{\partial V_{OC}}{\partial SoC}\frac{I_0}{Q_0^2} \end{bmatrix} \tag{3.13}$$

As we can see from the above equations if we linearize our model around a zero nominal current I_0, then our observability matrix is not full rank which implies that our system is unobservable. Also, if the slope $\frac{\partial V_{OC}}{\partial SoC}$ is extremely small we may potentially have observability issues. This analysis gives us insight into the fact that system observability is a challenge for estimation. For practical purposes, the estimation is performed when the battery is either being charged or discharged and hence we do not encounter this issue. It is however important to be aware of the observability conditions.

The next section explains the Least Squares Estimation algorithm and how it applies to our model.

3.5 Least Squares Estimation

Least Squares Estimation (LSE) technique is an extensively used technique in the adaptive control literature for system identification [38]. It is used to estimate parameters for a given system, using input(regressors) and output values(measurements). The method becomes simpler if it is used on a model which is linear in its parameters.

Below we will look at the derivation for least squares estimation and recursive least squares estimation .

The invention of least squares estimation is credited to Karl Friedrich Gauss[39]. Using it for astronomical studies, Gauss described the method of determining unknown parameters of a model by minimizing the sum of the squares of the differences between observed and computed value multiplied by numbers that measure degree of precision. Putting his statement in mathematical equations, we find that we have a system that can be written in the form

$$y(t) = \phi_1(t)\theta_1 + \phi_2(t)\theta_2 + ...\phi_n(t)\theta_n = \phi^T(t)\theta \tag{3.14}$$

where

$$\begin{aligned} &\phi^T = [\phi_1(1)\ \phi_2(2)\ \phi_3(3)\ ...\phi_n(t)] \\ &and \\ &\theta = [\theta_1\ \theta_2\ \theta_3\ ...\theta_n] \end{aligned} \tag{3.15}$$

In the above equation y is the measured variable (output) and the variables ϕ are called the regression variables or regressors (inputs). θ are the parameters being estimated and y is linear in θ. Now the purpose of a least squares estimator is to find the parameter set θ such that the following quadratic function, F is minimized

$$F(\theta, t) = \frac{1}{2}\sum_{t=1}^{n}(y(t) - \phi^T\theta)^2 \tag{3.16}$$

For the equation above, the minimum is obtained for parameters θ such that

$$\Phi^T\Phi\theta = \Phi^T Y \tag{3.17}$$

where

$$\Phi^T = [\phi(1)\ \phi(2)\ \phi(3)\ ...\phi(t)]\ \ and\ \ \ Y(t) = [y(1)\ y(2)\ y(3)\ ...y(t)]T \tag{3.18}$$

The minimum is then given by the estimate

$$\theta = (\Phi^T \Phi)^{-1} \Phi^T Y \tag{3.19}$$

Since, our purpose is to eventually apply the algorithm online, thereby reducing computing time and memory use, we look at recursively applying least squares estimate to the incoming measurements and obtaining parameters. The LSE can be discretized and arranged such that the results obtained till the previous time step can be used to get the new estimates at current time. Assuming that the matrix $\Phi^T \Phi$ is non-singular, we can define P(t) as

$$\begin{aligned} P^{-1}(t) &= \Phi^T \Phi \\ &= \sum_{t=1}^{n} \phi(t)\phi^T(t) \\ &= \sum_{t=1}^{n-1} \phi(t)\phi^T(t) + \phi(n)\phi^T(n) \\ &= P^{-1}(t-1) + \phi(n)\phi^T(n) \end{aligned} \tag{3.20}$$

Then, we can obtain P(t) as

$$\begin{aligned} &P(t) = P(t-1) * \left(I - \frac{\phi(n)\phi^T(n)P(t-1)}{1 + \phi^T(n)P(t-1)\phi(n)} \right) \\ &e(t) = (y(t) - \phi^T(t)\theta(t-1)) \\ &Then \\ &\theta(t) = \theta(t-1) + P(t)\phi(t)e(t) \end{aligned} \tag{3.21}$$

Thus we can obtain estimates recursively. Here *e(t)* can be interpreted as the error (residual) in the estimation. We use the above derived RLS for our purpose in the simulations.

In the next couple of sections we derive the Least Squares Estimator for our model and look at the problems that we may face in estimation.

3.6 Implementing LSE on our model

In the previous section we discussed the Least Squares Estimator and its application to parameter estimation. In our problem, we have two parameters, namely capacity and internal resistance that need to be estimated. We will formulate a LSE for the same. In the process we assume that at every point of time we can find the correct value of SoC. This is done using another estimator in parallel with the LSE. The gain for this is determined by running a simple Kalman Filter on just the SoC problem, assuming that we know the parameter values correctly. Once the gain is decided, a constant gain observer that is able to precisely estimate the State of Charge is implemented.

We will now move forward to deriving the equations for the LSE. Rewriting our model equations, under the assumption that the only state is SoC, while capacity and internal resistance are the parameters.

$$\begin{aligned} \dot{SoC} &= \frac{I}{Q} \\ V &= V_{OC}(SoC) + IR \end{aligned} \tag{3.22}$$

Linearizing output equation we get

$$V = \alpha SoC + IR \tag{3.23}$$

Here α is the linearization value of OCV around a particular value of SoC.
Discretizing the above equations

$$\begin{aligned} & SOC_k - SOC_{k-1} = \frac{I_k}{Q}\Delta t \\ & so \\ & SOC_k = SOC_{k-1} + \frac{I_k}{Q}\Delta t \\ & V_k = \alpha SoC_k + I_k R \\ & and \\ & V_{k-1} = \alpha SoC_{k-1} + I_{k-1} R \end{aligned} \tag{3.24}$$

Making substitutions and assuming that Δt is 1 second, we get

$$V_k - V_{k-1} = \alpha(SOC_k - SOC_{k-1}) + R(I_k - I_{k-1})$$
$$where$$
$$SOC_k - SOC_{k-1} = \frac{I_k}{Q}$$
$$Thus,$$
$$\delta V_k = \alpha\frac{I_k}{Q} + R(\delta I_k) \tag{3.25}$$

Now writing the final equation in LSE form we get

$$\begin{bmatrix} \delta V_1 \\ \delta V_2 \\ . \\ . \\ \delta V_n \end{bmatrix} = \begin{bmatrix} I_1 & \delta I_1 \\ I_2 & \delta I_2 \\ . & . \\ . & . \\ . & . \\ I_n & \delta I_n \end{bmatrix} \begin{bmatrix} \frac{\alpha}{Q} \\ R \end{bmatrix} \tag{3.26}$$

Or

$$\begin{bmatrix} \delta V_1 \\ \delta V_2 \\ . \\ . \\ \delta V_n \end{bmatrix} = \begin{bmatrix} \alpha I_1 & \delta I_1 \\ \alpha I_2 & \delta I_2 \\ . & . \\ . & . \\ . & . \\ \alpha I_n & \delta I_n \end{bmatrix} \begin{bmatrix} \frac{1}{Q} \\ R \end{bmatrix} \tag{3.27}$$

We can use any one of the above final equations for simulation. It has to be noted that α is the linearization of OCV around a value of SoC and this SoC is estimated as well. SoC is estimated using a constant gain observer continuously.

Further, we use recursive least squares (RLS) estimation, since we intend to implement the algorithm online and it reduces the computational time as well as memory required by the processor. As discussed in the previous section we can

apply the recursive LSE to a least squares problem, which is done in our case for simulation.

3.7 Persistence of Excitation

In the previous section we described the application of the LSE to our model. In this section we look at the estimator in terms of persistence of excitation. According to literature, a necessary condition for the system to be identifiable/observable is that the input signal should be persistently excited. In other words for persistent excitation (PE), the matrix $\phi(t)$ should be full rank and the matrix $\Phi^T\Phi$ should be invertible (non-singular)[38, 40].

If we carefully look at our ϕ matrix from the previous section we can see that there can exist conditions for which our system might not be persistently excited. The ϕ matrix that we obtained was

$$\phi = \begin{bmatrix} I_1 & \delta I_1 \\ I_2 & \delta I_2 \\ . & . \\ . & . \\ . & . \\ I_n & \delta I_n \end{bmatrix} \tag{3.28}$$

Most of the literature discussed in the previous chapter uses Constant Current Constant Voltage charge-discharge cycles for testing and validating either the models or the estimation algorithms used. CCCV cycling is one of the most commonly used techniques for testing Li-ion batteries has been Constant Current Constant Voltage charge-discharge cycles. Other methods applied also use a variation of the CCCV for testing. Either a constant current discharge or a constant current charge is used. Establishing the widespread use of this method, we see that if the current input is constant (during CC mode of charge/discharge) then our ϕ matrix becomes

$$\phi = \begin{bmatrix} I_1 & 0 \\ I_2 & 0 \\ . & . \\ . & . \\ . & . \\ I_n & 0 \end{bmatrix} \tag{3.29}$$

which implies that $\Phi^T\Phi$ is not full rank and hence the system if unidentifiable. This disables us from estimating the stated parameters. If we look at the CV part of the CCCV process we observe that the output vector y in the model becomes zero as show in equation 3.30. If the output vector is zero then we have an estimation problem in the form $\phi^T\theta = 0$ which has a solution only if ϕ is not full rank. Again we see that we cannot obtain our parameter values uniquely and thus estimation can't be performed.which again creates a problem in estimating our parameters.

$$\begin{bmatrix} \delta V_1 \\ \delta V_2 \\ . \\ . \\ \delta V_n \end{bmatrix} = \begin{bmatrix} 0 \\ 0 \\ . \\ . \\ . \\ 0 \end{bmatrix} \tag{3.30}$$

This analysis leads us to the conclusion that PE becomes important in the parameter estimation for Li-ion batteries. In particular, this affects the estimation of resistance as the vector that goes to zero is the regressor vector for estimating the internal resistance. This problem is addressed in the following chapter with the possibility of obtaining better estimates by adding persistent dither to the input. The dither added is an independent and identically distributed random variable with zero mean. This dither is added to the input going to the system, hence the estimator is aware of the characteristics of the dither noise being added.

In the next section we look at the OCV-SoC curve flatness and issues associated with it.

3.8 Flatness of OCV-SOC curve

As discussed in the previous sections, the estimation of capacity and resistance is highly dependent on the knowledge of SoC estimate accurately. In our model, we linearize the output equation to obtain α, which signifies the slope of the OCV-SoC curve at the particular instant of estimation. As can be seen from the figure shown earlier, the curve is extremely flat around the 20-80% region, i.e. the battery undergoes a significant change in state of charge with the voltage changing by a few fractions of a volt in comparison. This flatness of the curve has been studied and possible solutions have also been presented, as explained in the literature earlier. The curve's relatively flat shape around the 20-80% SoC region makes the estimation problem difficult if the only measurements are current and voltage. We intend to derive the variation in the estimation of capacity with respect to the slope of the OCV-SoC curve to study this dependence.

From the estimation literature, we know that the covariance of the estimate θ is dependent on the noise in measurements (zero mean and variance σ^2) as

$$\begin{aligned} cov(\theta) &= \sigma_V^2[\Phi^T\Phi]^{-1} \\ &= \sigma_V^2\begin{bmatrix} \overrightarrow{I^T}\overrightarrow{I} & \overrightarrow{I^T}\overrightarrow{\delta I} \\ \overrightarrow{(\delta I)^T}\overrightarrow{I} & \overrightarrow{(\delta I)^T}\overrightarrow{\delta I} \end{bmatrix}^{-1} \end{aligned} \tag{3.31}$$

The matrix inverse

$$M^{-1} = \begin{bmatrix} \overrightarrow{I^T}\overrightarrow{I} & \overrightarrow{I^T}\overrightarrow{\delta I} \\ \overrightarrow{(\delta I)^T}\overrightarrow{I} & \overrightarrow{(\delta I)^T}\overrightarrow{\delta I} \end{bmatrix}^{-1} = \frac{\begin{bmatrix} \overrightarrow{(\delta I)^T}\overrightarrow{\delta I} & -\overrightarrow{I^T}\overrightarrow{\delta I} \\ -\overrightarrow{(\delta I)^T}\overrightarrow{I} & \overrightarrow{I^T}\overrightarrow{I} \end{bmatrix}}{\sigma_V^2 D} \tag{3.32}$$

Here D is the determinant of the matrix M. Thus now our covariance becomes

$$cov(\theta) = \sigma_V^2\frac{\begin{bmatrix} \overrightarrow{(\delta I)^T}\overrightarrow{\delta I} & -\overrightarrow{I^T}\overrightarrow{\delta I} \\ -\overrightarrow{(\delta I)^T}\overrightarrow{I} & \overrightarrow{I^T}\overrightarrow{I} \end{bmatrix}}{\sigma_V^2 D} \tag{3.33}$$

Now θ contains both of our parameters

$$\theta = \begin{bmatrix} \frac{\alpha}{Q} \\ R \end{bmatrix} \tag{3.34}$$

Separating the covariance of capacity from resistance we get

$$cov(\frac{\alpha}{Q}) = \frac{\left[\overrightarrow{(\delta I)^T}\overrightarrow{\delta I}\right]}{\sigma_V^2 D} \tag{3.35}$$

The Left Hand Side (LHS) of the above equation yields

$$cov(\frac{\alpha}{Q}) = E\left\{\left[\left(\frac{\alpha}{Q}\right)_{est} - \left(\frac{\alpha}{Q}\right)_{act}\right]^2\right\} \tag{3.36}$$

where $\left(\frac{\alpha}{Q}\right)_{est}$ is the estimated value and $\left(\frac{\alpha}{Q}\right)_{act}$ is the actual value of the parameter.

Then, writing the estimate as

$$Q_{est} = Q + \delta Q \tag{3.37}$$

we get

$$E\left\{\left[\left(\frac{\alpha}{Q}\right)_{est} - \left(\frac{\alpha}{Q}\right)_{act}\right]^2\right\} = E\left\{\left[\left(\frac{\alpha}{Q+\delta Q}\right) - \left(\frac{\alpha}{Q}\right)\right]^2\right\} \tag{3.38}$$

Approximating using Taylor series expansion we get,

$$\begin{aligned} E\left\{\left[\left(\frac{\alpha}{Q+\delta Q}\right) - \left(\frac{\alpha}{Q}\right)\right]^2\right\} &\approx E\left\{\left[\left(\frac{\alpha}{Q}\right) - \left(\frac{\alpha}{Q^2}\right)\delta Q - \left(\frac{\alpha}{Q}\right)\right]^2\right\} \\ &\approx E\left[\frac{\alpha^2}{Q^4}(\delta Q)^2\right] \\ &\approx \frac{\alpha^2}{Q^4}E\left[(\delta Q)^2\right] \\ &= \frac{\alpha^2}{Q^4}cov(\delta Q) \end{aligned}$$

Substituting this back into earlier equations we get

$$\sigma_V^2 \frac{\overrightarrow{(\delta I)^T}\overrightarrow{\delta I}}{D} = \frac{\alpha^2}{Q^4} cov(\delta Q)$$

$Thus,$

$$cov(\delta Q)^2 = \frac{Q^4 \sigma_V^2 \overrightarrow{(\delta I)^T}\overrightarrow{\delta I}}{\alpha^2 D} \tag{3.39}$$

As stated in the above relation the covariance of the change in capacity estimation varies inversely as the square of the slope of the OCV-SoC curve.

$$cov(\delta Q)^2 \propto \frac{1}{\alpha^2} \tag{3.40}$$

This derivation gives us insight into the capacity estimation problem. If the estimation is done around the flat region of the curve, the slope is negligible and hence the estimate will not be accurate and might not even converge. However, if we try to estimate around higher slope value (0-20% or 80-100%) regions, we might be able to get a better estimate. This idea is further discussed and implemented in the next chapter. Thus, the OCV-SoC slope is also identified as a challenge in combined SoC-SoH estimation. we apply Cramér-Rao bounds to our least sqaures estimator to further solidify our claims of potential challenges.

3.9 Cramér-Rao Bounds

For any unbiased parameter estimator, the Cramér-Rao bounds are used to determine the minimum error values, by setting a lower bound on the second order moments[41]. For our estimator we derive a form of the Cramér-Rao bounds to provide insight into the limiting factors for the parameters we are trying to estimate.

Our model is given by the linearized set of equations

$$\dot{SoC} = \frac{I}{Q}$$
$$V = \alpha SoC + IR \tag{3.41}$$

Our state equation can be discretized as follows, assuming zero-order hold,

$$SoC = SoC_0 + \frac{1}{Q}\sum_{i=1}^{t} I \tag{3.42}$$

Substituting this in our output equation we get

$$V = \alpha SoC_0 + \frac{\alpha}{Q}\sum_{i=1}^{t} I + R * I \tag{3.43}$$

To get the Cramér-Rao bounds, we first have to find the Fisher information matrix. For this we have to find the partial derivative of the output with respect to the parameters.

$$\frac{\partial V}{\partial R} = I \tag{3.44}$$

and

$$\frac{\partial V}{\partial Q} = \frac{-\alpha}{Q^2}\sum_{i=0}^{t} I \tag{3.45}$$

Hence we can get a vector as

$$\frac{\partial \overrightarrow{V}^T}{\partial \theta} = \begin{bmatrix} I_1 & I_2 & ... & I_t \\ \frac{-\alpha}{Q^2} I_1 & \frac{-\alpha}{Q^2}(I_1 + I_2) & ... & \frac{-\alpha}{Q^2}(I_1 + I_2 ... I_t) \end{bmatrix} \tag{3.46}$$

Let $\overrightarrow{I}$ be the vector

$$\overrightarrow{I} = \begin{bmatrix} I_1 & I_2 & I_3 & . & . & I_t \end{bmatrix} \tag{3.47}$$

Furthermore, let $\overrightarrow{\sum I}$ be the vector,

$$\overrightarrow{\sum I} = \begin{bmatrix} I_1 & I_1 + I_2 & I_1 + I_2 + I_3 & ... & ... & I_1 + I_2 + I_3 + ...I_t \end{bmatrix} \tag{3.48}$$

The Fisher information matrix, under the assumption that the measurement noise is Gaussian with standard deviation σ ,is

$$F = \frac{1}{\sigma_V^2}[\frac{\partial \overrightarrow{V}}{\partial \theta}]^T[\frac{\partial \overrightarrow{V}}{\partial \theta}] \tag{3.49}$$

$$\tag{3.50}$$

$$= \frac{1}{\sigma^2}\begin{bmatrix} \overrightarrow{I}^T\overrightarrow{I} & \frac{-\alpha}{Q^2}\overrightarrow{I}^T\overrightarrow{\sum I} \\ \frac{-\alpha}{Q^2}\overrightarrow{I}^T\overrightarrow{\sum I} & \frac{\alpha^2}{Q^4}\overrightarrow{\sum I}^T\overrightarrow{\sum I} \end{bmatrix} \tag{3.51}$$

If we look at the term $\frac{-\alpha}{Q^2}\overrightarrow{I}^T\overrightarrow{\sum I}$ in the Fisher information matrix, we can prove that it is equal to zero for complete battery cycles.

$$\begin{aligned} \frac{-\alpha}{Q^2}\overrightarrow{I}^T\overrightarrow{\sum_{i=1}^{t} I} &= \frac{-\alpha}{Q^2}(I_1(I_1) + I_2(I_1 + I_2) + ...I_t(I_1 + I_2 + ...I_t)) \\ &= \frac{-\alpha}{Q^2}\sum_{i=1}^{t} I_i(\sum_{j=1}^{i} I_j) \end{aligned} \tag{3.52}$$

We know that

$$\sum_{j=1}^{i} I_j = Q * (SoC - SoC_0) = Q * \frac{V - V_0}{\alpha} \tag{3.53}$$

Substituting this back in equation 3.52, we obtain

$$\begin{aligned} \frac{-\alpha}{Q^2}\overrightarrow{I}^T\overrightarrow{\sum_{i=1}^{t} I_i} &= \frac{-\alpha}{Q^2}\sum_{i=1}^{t} I_i * Q * \frac{(V_i - V_0)}{\alpha} \\ &= \frac{-1}{Q}(\sum_{i=1}^{t} I_i V_i - \sum_{i=1}^{t} I_i V_0) \end{aligned} \tag{3.54}$$

$\sum_{i=1}^{t} I_i V_i$ represents the amount of energy into and out of the battery's internal capacitance which is zero over a cycle according to the law of conservation of energy. $\sum_{i=1}^{t} I_i V_0$ is zero over a cycle as well, due to conservation of charge. Then we obtain,

$$\frac{-\alpha}{Q^2}\overrightarrow{I}^T\overrightarrow{\sum_{i=1}^{t} I} = 0 \tag{3.55}$$

Now if we look at our Fisher information matrix we get

$$F = \frac{1}{\sigma^2}\begin{bmatrix} \overrightarrow{I}^T\overrightarrow{I} & 0 \\ 0 & \frac{\alpha^2}{Q^4}\overrightarrow{\sum I}^T\overrightarrow{\sum I} \end{bmatrix} \tag{3.56}$$

Then we get the Cramér-Rao bounds as

$$C_{bound} \geq \sigma^2\begin{bmatrix} (\overrightarrow{I}^T\overrightarrow{I})^{-1} & 0 \\ 0 & (\frac{\alpha^2}{Q^4}\overrightarrow{\sum I}^T\overrightarrow{\sum I})^{-1} \end{bmatrix} \tag{3.57}$$

The bounds for individual parameter errors are

$$C_{resistance} \geq \frac{\sigma^2}{\overrightarrow{I}^T\overrightarrow{I}} \tag{3.58}$$

and

$$\frac{C_{capacity}}{Q^2} \geq \frac{\sigma^2 Q^2}{\alpha^2 \overrightarrow{\sum I^T} \overrightarrow{\sum I}} \tag{3.59}$$

The bounds that we thus obtain give us another insight into the dependency of the estimation errors of both the parameters.

The resistance estimation error is dependent on the noise of the sensors and is inversely related to the value of current. This means that for higher values of current we can obtain better estimates of resistance.

The capacity estimation error is highly dependent on the slope of the OCV-SoC curve, which reiterates what we mentioned earlier. The smaller the value of the slope, the higher is our error in estimation. Also it depends on accurately knowing the value of SoC at all times.

The next chapter explains the various simulation studies done to support the mathematical derivations done in this chapter. Simulations are done by varying different parameters including but not limited to PE dither and slope of OCV-SoC curve to understand their significance in the estimation problem. Monte-Carlo simulations are done eventually to study the trade-offs between various parameters.

Chapter 4

Simulation Results and Discussion

4.1 Introduction

Chapter 3 went through a simple equivalent circuit model and mathematical analysis for identifying key challenges with combined SoC-SoH estimation. This was done by exploring the problem from three perspectives, namely, Extended Kalman Filter, Least Squares Estimation and the Cramér-Rao bounds. All the three methods are different in their approach but give potentially the same conclusions. Two main challenges related to identifiability of estimation parameters were determined :

- Capacity Estimation is dependent on the OCV-SoC slope and region of operation
- Resistance Estimation is dependent on persistence excitation of the input

This chapter demonstrates the above feelings via simulations. For capacity estimation, various regions of the OCV-SoC curve are examined to show that higher slopes give better estimates. For resistance estimation, the PE dither added to the input is increased from 0.001A to 0.1 A to show the decrease in estimation error. The chapter examines the effects of PE dither and OCV-SoC slope using single focused simulation studies first. This is useful for gaining preliminary insights, but raises the question of how repeatable the simulation results are for different realizations of the stochastic noise and dither signals. To address this repeatability

issue, the author performs Monte-Carlo simulations of the least squares estimator under consideration. These Monte-Carlo simulations provide further insights into the effects of PE dither, OCV-SoC curve flatness, sensor noise, initial estimation error, and time on the proposed estimator's accuracy. The author emphasizes the fact that the estimation of SoC and SoH is done simultaneously with no offline estimation, hence the three estimates, state of charge, capacity and resistance are constantly interacting and being updated.

It should be noted that inherently the recursive least squares estimation algorithm produces very high errors at the beginning of estimation. This is because the algorithm requires a choice of initial covariance matrix. This choice of covariance matrix corresponds to a trade-off between estimator speed and accuracy. Thus a value is chosen carefully for relatively fast estimation at the sake of high initial error. Hence, it is important to collect 1-2 hours worth of data before treating the parameter estimates as potentially accurate. This is the reason why we assess our estimator performance based on its behavior after this initial transient period. If we take a baseline case with conditions described in Table 4.4 then we obtain Figure 4.1 which shows the percentage error in parameter estimation. The figure confirms the importance of avoiding the first few cycles of simulation due to high error percentage and the need to wait for the transients to die before beginning estimation.

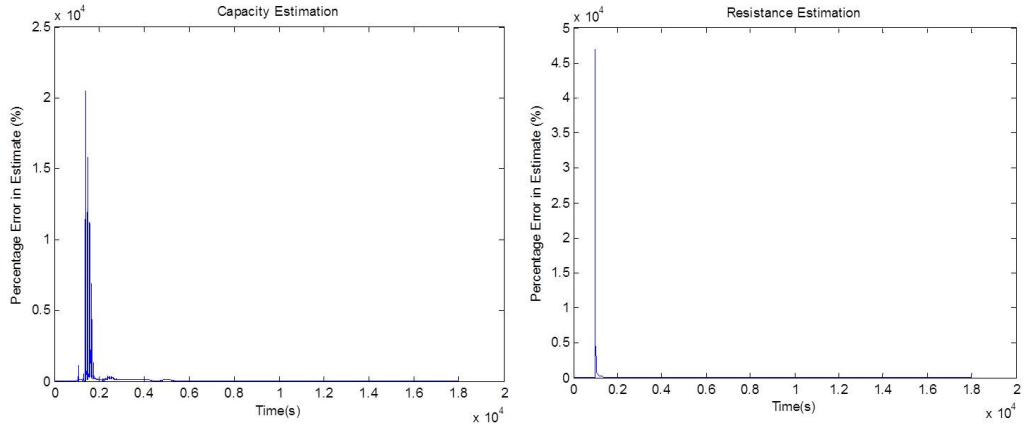

Figure 4.1. Estimation Error for Entire Simulation Time

To verify the conclusion made via mathematical analysis in the previous chapter, we study the effect of PE dither on resistance estimation and OCV-SoC slope on capacity estimation in Sections 4.2 and 4.3. We also look at SoC estimation, being performed simultaneously, in Section 4.4. As stated earlier, Monte-Carlo simulations are performed where different parameters of simulation namely, PE dither, OCV-SoC region, measurement noise, duration of simulation and initial conditions are individually varied to study their effect on estimation. This is done in Section 4.5, to solidify the claims(conclusions) made in Sections 4.2 and 4.3. Finally a brief conclusion is made to reinstate the developments done in this chapter.

The next section describes the persistent excitation problem and illustrates the effect of adding dither to the input signal.

4.2 Persistence of Excitation

As discussed in the previous chapter, the CC and CV parts of the charge-discharge cycle are inherently not persistently exciting. Thus, it becomes imperative to make sure that the input signal to the plant is able to produce estimates at all times. A solution to this problem is to add dither to the input signal. Adding a small dither to the signal will make it persistently exciting at all times, thus making it possible to estimate the parameters at every time step. The dither amplitude may be very low (as low as 10% of actual noise in input) or high (as much as 10 times the level of noise). The amplitude of the dither also has an effect on the accuracy of estimation of the parameters.

Below we demonstrate a case where two different dither signals are added to exactly the same model and under same conditions.

The battery undergoes a CCCV charge-discharge cycle continuously with the simulation conditions listed in Table 4.1.

The error percentages shown are for the last 4 hours of simulation. The two dither amplitudes used are 1mA (10% of sensor noise) and 100mA (10 times sensor noise), to show the vast difference in corresponding estimate errors. We obtain the results illustrated in Figures 4.2 and 4.3.

As we can see from the figures, the estimation error is very small in the simulation with higher PE dither. This supports our hypothesis of the effect of PE noise

Table 4.1. Simulation Conditions for Persistence of Excitation

Simulation Time (hours)	5
Time Step (seconds)	1
Standard Deviation in Current Sensor Noise,σ_I (A)	0.01
Standard Deviation in Voltage Sensor Noise,σ_V (V)	0.0015
SoC Range (%)	20-80
Initial SoC Error(%)	50
Initial Capacity Error(%)	10
Initial Resistance Error(%)	10

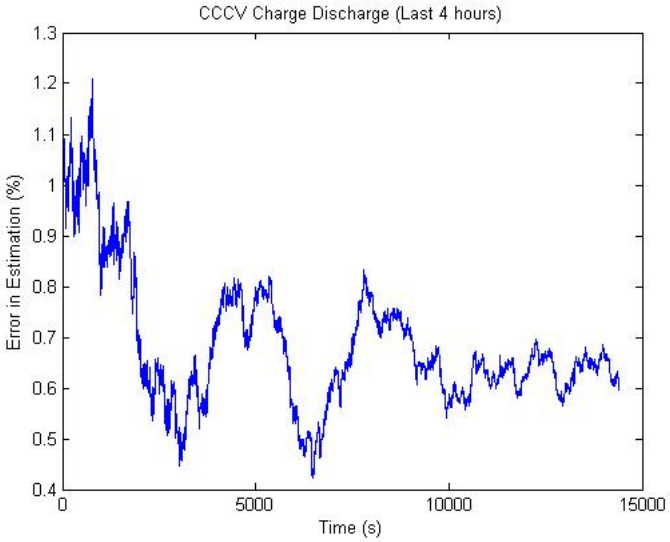

Figure 4.2. 100 mA PE Dither for Resistance Estimation

on the estimation of resistance. As explained in the previous chapter, the lack of persistence of excitation leads to a bad estimate of resistance. As we increase the dither added to the input signal we obtain a better estimate. A trade-off between increasing dither values and error in estimation is studied via Monte Carlo simulations and the average estimation error value alongwith the standard deviation is calculated. This is discussed in the following sections.

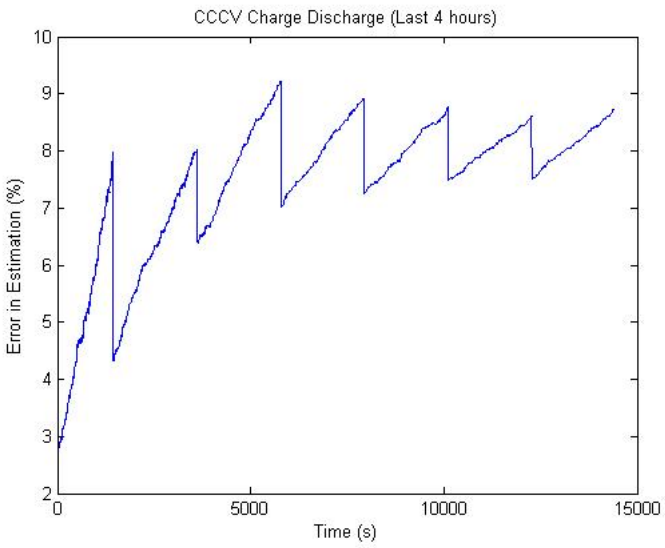

Figure 4.3. 1 mA PE Dither for Resistance Estimation

4.3 OCV-SoC Curve Flatness

The open circuit voltage is linearized around a nominal SoC at every time step in the estimation of capacity. The SoC is obtained via another estimator in parallel. However, the slope of the curve is important to predict capacity accurately. The effect of the slope is studied in this section. As can be seen from the OCV-SoC curve the flat region is usual region of operation for the battery. However the slope is really high around the edges and these two cases are considered for comparison in this section. The first simulation is done for the 20-80% range of SoC and the second simulation is done for 0-100% range. The other simulation parameters are listed in Table 4.2.

Using these parameter, we obtain the error estimates for capacity as shown in Figure 4.4 and 4.5.

The figures clearly show the difference in error percentages when simulated for different SoC ranges. The error in estimating capacity over a higher SoC range which includes very steep slopes (0-100%) is far lesser than those obtained over a smaller range (20-80%).

As mentioned earlier the slope plays an important role in capacity estimation because it is linked to OCV-SoC curve of the battery. The OCV-SoC curve of

Table 4.2. Simulation Conditions for OCV-SoC Curve Flatness

Simulation Time (hours)	5
Time Step (seconds)	1
Standard Deviation in Current Sensor Noise,σ_I (A)	0.01
Standard Deviation in Voltage Sensor Noise,σ_V (V)	0.0015
PE Dither (A) (%)	0.001
Initial SoC Error(%)	50
Initial Capacity Error(%)	10
Initial Resistance Error(%)	10

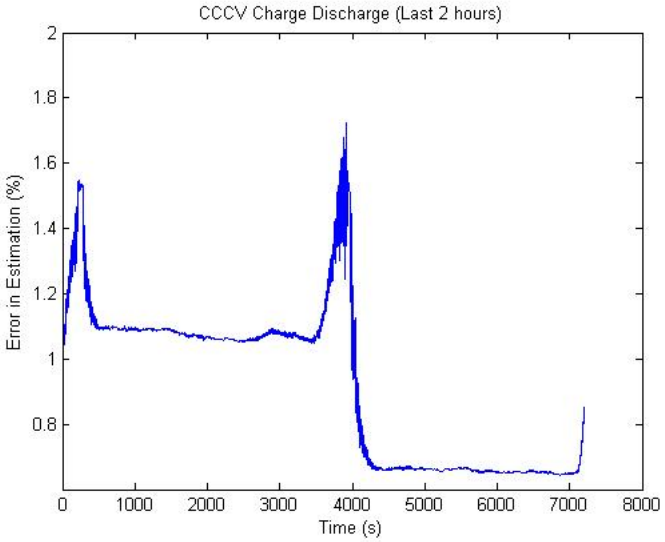

Figure 4.4. Capacity Estimation Error for 0-100% SoC Range

the battery changes as the capacity changes and hence determining the value of slope at any given point of time in the battery's life is important for the estimation of capacity. The voltage and current values are the only measurements made for estimation and since the voltage remains steady for a major part of the SoC region, the ends of the slope become significant.

The simulation done above is for a very small dither amplitude and for two regions of SoC. In most practical cases, the full range of the voltage of a battery

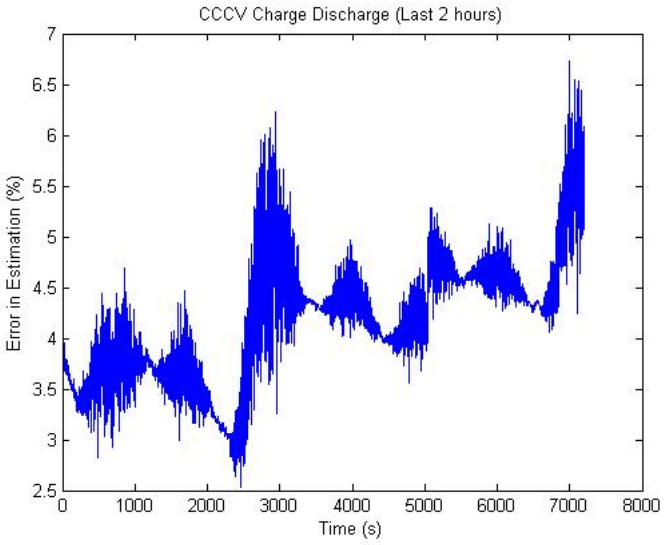

Figure 4.5. Capacity Estimation Error for 20-80% SoC Range

is not used and hence it is important to see the effect of different dither amplitudes and different SoC regions on parameter estimation. This is done in the next sections.

4.4 SoC Estimation

This thesis concentrates on simulatenouely estimating the state of charge and health parameters. Throughout the simulations performed, SoC of the battery is continuously monitored using the measurements combined with a constant gain observer. The estimate of the SoC is used to do all the simulations. At no point of time in the entire process does the system know of the real SoC. This adds another dimension to the existing problem as the initial error in SoC leads to high estimation errors in both capacity and resistance due to the inter-dependence of all three, as can bee seen by the system equations described earlier. In order to show that the estimation of SoC is done accurately Figures 4.6 and 4.7 are obtained. The simulations are done for a period of 8 hours to show consistency. Parameters are listed in 4.3.

The figures mentioned above show the SoC over an 8 hour period, and it can be seen that the estimation is very accurate, even after being set off from the original

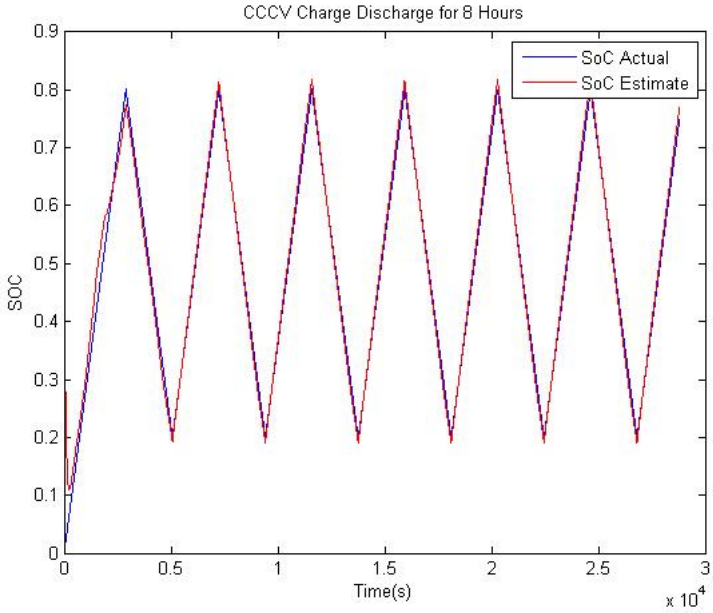

Figure 4.6. SoC Estimation for 20-80% SoC Range

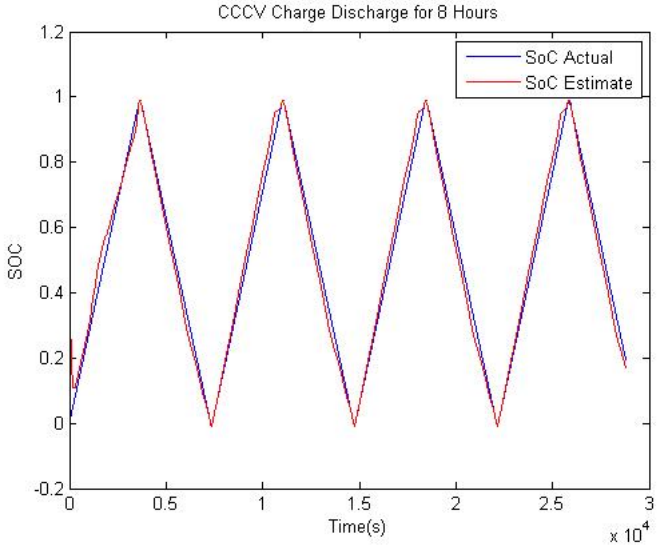

Figure 4.7. SoC Estimation Error for 0-100% SoC Range

Table 4.3. Simulation Conditions for SoC Estimation

Simulation Time (hours)	8
Time Step (seconds)	1
Standard Deviation in Current Sensor Noise,σ_I (A)	0.01
Standard Deviation in Voltage Sensor Noise,σ_V (V)	0.0015
PE Dither (A) (%)	0.02
Initial SoC Error(%)	50
Initial Capacity Error(%)	10
Initial Resistance Error(%)	10

vale by as much as 50%.

In the next section, we discuss the trade-offs involved with the combined SoC-SoH estimation problem.

4.5 Trade-Offs using Monte-Carlo Simulations

To study the trade-off and understand the effect of varying different simulation conditions we perform a series of different tests. The simulations done in the previous sections were very particular in their conditions and repeatability could be a potential problem. Hence to perform a rigorous statistical analysis, we perform each of the simulation 100 times. This gives us a good sample space for calculating the mean and standard deviation in the estimation errors. The number of simulations was decided after repeating the experiments for 1, 50, 100 and 1000 times and calculating the statistics. It was observed that 100 simulations created a sample space enough for the estimates to converge. also, the error percentages are shown after the error reaches steady state. We obtain a standard set of simulation conditions listed in 4.4. In the next sections we vary each parameter in the table and study its effect on the estimation error.

Table 4.4. Simulation Conditions for Monte-Carlo

Simulation Time (hours)	5
Time Step (seconds)	1
Standard Deviation in Current Sensor Noise,σ_I (A)	0.01
Standard Deviation in Voltage Sensor Noise,σ_V (V)	0.0015
PE Dither (A)	0.02
SoC Range (%)	20-80
Initial SoC Error(%)	50
Initial Capacity Error(%)	10
Initial Resistance Error(%)	10

4.5.1 Effect of PE Dither

Monte-Carlo simulations are done by varying the dither value from 1mA to 100mA keeping other simulation conditions the same. We start by varying dither amplitude to study its effect on estimation. For every dither value, 100 simulations are done and the mean error percentage is calculated. Also the standard deviation of the error is calculated and plotted. These results are shown in Figure 4.8 for both the SoC ranges (0-100% and 20-80%)

The results presented are interesting for a few deductions. In the resistance estimation plot we can see that for both the SoC ranges we get a better resistance estimation as the dither amplitude increases. This is coherent with our hypothesis on the importance of dither in resistance estimation. We can also see that for the different ranges of SoC there is a large variation in the estimation of R. The 20-80% region gives significantly better results than the 0-100% SoC range. This is because, in the flat operating region the change in current due to the dither has a significantly larger effect on the voltage values and hence the resistance is estimated well. In the higher regions of SoC, the change in voltage is high for small changes in SoC and this overshadows the effect of dither and hence resistance is not estimated correctly. However, if we increase the dither value, we observe that the resistance becomes better as the effect of dither influences the voltage change

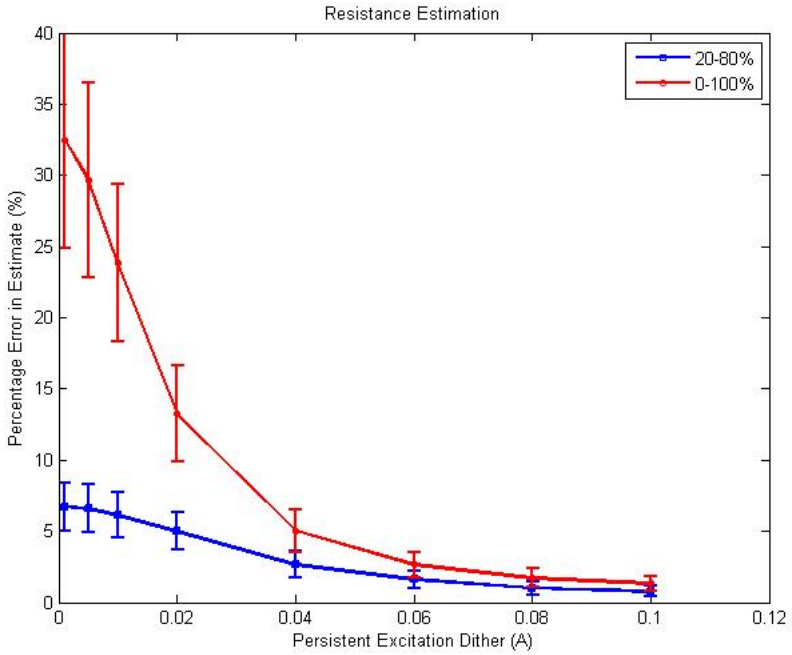

Figure 4.8. Monte-Carlo Simulations for Resistance Estimation

more. We can see from the figire that for PE dither 0.06A or above the estimation error percentage for resistance falls below 5%, which is an acceptable amount of error for resistance.

Figure 4.9 shows the average error in capacity for different dither and SoC range values. As expected, the 0-100% range has a far better estimation capability than the 20-80% range. The dither amplitude does not have a very significant effect on the capacity estimation. We see that the error in capacity for 0-100% region is always in the 2% region whereas for 20-80% range it is as high as 10% of total capacity. Since in general cases, a battery is declared 'dead' once it reaches 80% (error of 20% in estimation) of its total capacity, a 10% error is very high. Thus we should prefer the 0-100% range for estimation. We also look at the combined error for both the estimates in Figure 4.10

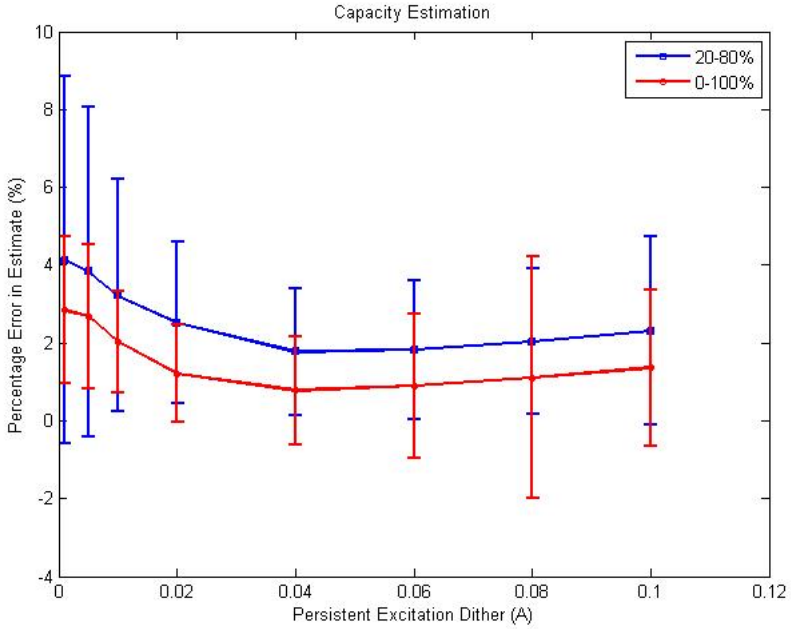

Figure 4.9. Monte-Carlo Simulations for Capacity Estimation

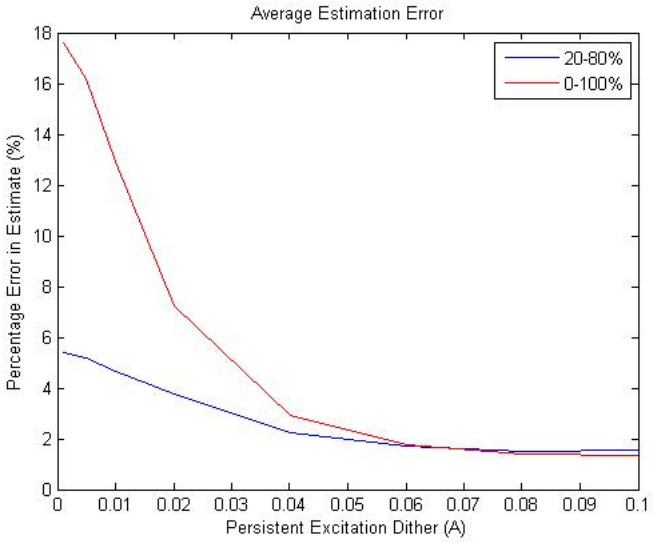

Figure 4.10. Monte-Carlo Simulations for Average Error

4.5.2 Effect of OCV-SoC curve flatness

We further explore the effect of varying the region of operation (SoC) on the estimation of capacity. We obtain the results listed in Table 4.5. E_{Qmean}, E_{Rmean}, σ_Q and σ_R are the mean of capacity estimation error, mean of resistance estimation error, standard deviation in capacity estimation error and standard deviation of resistance estimation error respectively. All the terms stated above are expressed in percentages. These terminologies will also be used in the further studies as well.

Table 4.5. Results for varying SoC regions

SoC Region (%)	E_{Qmean} (%)	E_{Rmean} (%)	σ_Q (%)	σ_R (%)
0-100	1.204	13.229	1.256	3.367
20-80	2.508	5.009	2.073	1.352
30-70	10.173	3.568	6.793	1.156

The results solidify the hypothesis that higher SoC-OCV regions with greater changes in slope lead to a better estimate of capacity. The important takeaway is to notice that there is a difference of magnitude in the error estimation as we move from 30-70% from 0-100%. However, it is not always possible to use the entire range for practical purposes, so we choose a SoC region where the error is limited. We have chosen the range of 20-80% for our further studies.

4.5.3 Effect of Sensor(Measurement) Noise

In our simulations till now we have assumed a constant value of sensor noise derived from our experiments. It may so happen that the sensors used practically may have better or worse noise characteristics. For high fidelity purposes, where cost is not a major issue, the sensors used will be of better standards, leading to lesser noise. On the other hand, for use in online mass production applications, where overall cost,space and other sources of noise might be an issue, the sensor noise might be more than that obtained through the lab experiment. Hence we look at the effect of different noise levels on the estimation problem.

We use three different noise levels other than the one demonstrated earlier. We simulate a zero noise condition, noise level half of original and a noise level

double of the originally obtained values. These results are tabulated in Table 4.6. It should be noted that the noise values in the table are in fact the standard deviation values for the measurement noises of current and voltage.

Table 4.6. Results for varying Sensor Noise

$\sigma_I(mA)$	$\sigma_V(mV)$	E_{Qmean} (%)	E_{Rmean} (%)	σ_Q (%)	σ_R (%)
0	0	0.668	1.010	0.490	0.216
5	0.75	0.702	0.753	0.493	0.338
10	1.5	2.071	5.579	1.221	0.781
15	2.25	11.732	12.730	9.757	1.213

If we have perfect sensors and our measurements are clean then we see that the error levels are reduced to negligible. However, it is interesting to see that a reduction in noise levels by half leads to a significant drop in the error values. Also, an increase in the noise levels to double their existing values leads a a substantial increase in the error percentages. This is in accordance with the belief that low sensor noise is imperative for better estimation.

We choose the experimentally obtained noise levels for our further studies as these give relatively sound error levels.

4.5.4 Varying the time duration of simulation

Till now our simulation has been for a 5 hour time span, so we look at other time spans in order to make sure that our estimator works for lower time intervals. Also, we want to see that given persistence excitation the least sqaures estimation algorithm guarantees that the estimation error converges to zero over an infinite period of time. We simulate our system for 4, 5 and 6 hour time intervals to show the progressive decline in estimation error.

The results are listed in Table 4.7

4.5.5 Varying initial conditions

The initial conditions determine how sure we are for our first guess for the parameters. These are changed to show how they affect the estimation results. The

Table 4.7. Results for varying time duration of simulation

Time Interval (hours)	E_{Qmean} (%)	E_{Rmean} (%)	σ_Q (%)	σ_R(%)
4	5.794	5.415	10.948	4.617
5	2.508	5.009	2.073	1.352
6	1.910	5.300	1.136	0.932

capacity and resistance estimates are set to be off by 20%, 10% and 1% of the actual values, to study the effect of varying the initial conditions.

The results obtained form the set of simulations are listed in Table 4.8. We observe that a change in initial estimate of capacity has a great effect on its estimation error, whereas the resistance is not affected as much by the initial conditions.

Table 4.8. Results for varying initial conditions

% Initial Error	E_{Qmean} (%)	E_{Rmean} (%)	σ_Q (%)	σ_R(%)
1	2.329	5.608	1.399	0.819
10	2.508	5.009	2.073	1.352
20	31.529	4.760	14.080	1.437

The simulation studies done in this chapter illustrate the fundamental challenges with SoC-SoH estimation in relation to factors such as PE dither, OCV-SoC region, sensor noise, time duration and initial conditions . The above analysis acts as a precursor to better understanding the design of estimators and can thus be helpful in making choices for a better combined estimator.

We are able to conclude from the simulation that an increase in PE dither helps us give more accurate resistance estimates(below 5% error). Similarly if we consider the higher regions of the OCV-SoC curve then we are able to estimate capacity better(below 2% error).

Chapter 5

Conclusion

In this thesis, the challenges pertaining to the combined SoC-SoH estimation for Li-ion batteries are addressed. The literature is surveyed for existing algorithms and models for determining health characteristics online. An equivalent circuit model is chosen for simulating the battery dynamics, due to the simplicity of implementation and its ability to capture the battery behavior relatively well. Key identifiability issues such as sensor noise, flatness of OCV-SoC curve and persistence of excitation in input signal (using CCCV cycles) are noticed.

Conditions for parameter identifiability and their effects on SoH prediction are derived using the extended Kalman filter, least squares estimation and Cramér-Rao bounds. The least squares algorithm is used recursively for computational ease to show the effects of varying parameters on the estimation problem. The importance of adding PE dither to the input to enhance resistance estimation is analysed mathematically and verified via simulations. Variation in OCV-SoC region is considered to study its effect on the capacity estimate and mathematical derivations combined with simulation studies show that better estimation is obtained if the ends of the OCV-SoC curve are included. Further the robustness of the results is checked by performing Monte-Carlo simulations to study the effect of each simulation condition (PE dither, OCV-SoC region, measurement noise, duration of simulation and initial conditions) on the entire system. The results obtained reiterate the importance of better sensors(measurement noise), slow rate of initial convergence (duration of simulation) and approximate knowledge of estimates (initial conditions). Thus a design problem for estimation is examined in the

thesis and the challenges faced by simultaneous SoC and SoH diagnosis, prognosis and control for on board applications are studied.

The above work can be further extended to incorporate the effect of many other external factors on the estimation error. Temperature is an important factor to be considered for onboard applications as the behavior of Li-ion batteries is highly sensitive to temperature gradients. The above study establishes the need for understanding the inherent challenges with battery testing via CCCV cycles. The issues listed should be considered while subjecting the batteries to long term health tests. The discussions serve as precursors to the design of a better algorithm/estimator for predicting battery health. Choosing different operating conditions based on the requirement of the application becomes imperative and is described in the thesis.

An algorithm designed taking the above measures into account and possessing the capability to prognose failure and eventual battery death can thus be established.

Bibliography

[1] Winter, M. and R. Brodd (2004) "What are batteries, fuel cells, and supercapacitors?" *ChemInform*, **35**(50), pp. no–no.

[2] Affanni, A., A. Bellini, G. Franceschini, P. Guglielmi, and C. Tassoni (2005) "Battery choice and management for new-generation electric vehicles," *Industrial Electronics, IEEE Transactions on*, **52**(5), pp. 1343–1349.

[3] Wood, E., M. Alexander, and T. Bradley (2011) "Investigation of battery end-of-life conditions for plug-in hybrid electric vehicles," *Journal of Power Sources*.

[4] Lukic, S., J. Cao, R. Bansal, F. Rodriguez, and A. Emadi (2008) "Energy storage systems for automotive applications," *Industrial Electronics, IEEE Transactions on*, **55**(6), pp. 2258–2267.

[5] Zhang, J. and J. Lee (2011) "A review on prognostics and health monitoring of Li-ion battery," *Journal of Power Sources*.

[6] Hu, X., S. Li, and H. Peng (2011) "A comparative study of equivalent circuit models for Li-ion batteries," *Journal of Power Sources*.

[7] Plett, G. (2004) "Extended Kalman filtering for battery management systems of LiPB-based HEV battery packs-Part 3. State and parameter estimation," *Journal of Power sources*, **134**(2), pp. 277–292.

[8] ——— (2004) "Extended Kalman filtering for battery management systems of LiPB-based HEV battery packs:: Part 1. Background," *Journal of Power sources*, **134**(2), pp. 252–261.

[9] ——— (2004) "Extended Kalman filtering for battery management systems of LiPB-based HEV battery packs:: Part 2. Modeling and identification," *Journal of power sources*, **134**(2), pp. 262–276.

[10] Ng, K., C. Moo, Y. Chen, and Y. Hsieh (2009) "Enhanced coulomb counting method for estimating state-of-charge and state-of-health of lithium-ion batteries," *Applied energy*, **86**(9), pp. 1506–1511.

[11] Piller, S., M. Perrin, and A. Jossen (2001) "Methods for state-of-charge determination and their applications," *Journal of Power Sources*, **96**(1), pp. 113–120.

[12] Codeca, F., S. Savaresi, and G. Rizzoni (2008) "On battery state of charge estimation: A new mixed algorithm," in *Control Applications, 2008. CCA 2008. IEEE International Conference on*, IEEE, pp. 102–107.

[13] Kozlowski, J., C. Byington, A. Garga, M. Watson, and T. Hay (2001) "Model-based predictive diagnostics for electrochemical energy sources," in *Aerospace Conference, 2001, IEEE Proceedings.*, vol. 6, IEEE, pp. 3149–3164.

[14] Chaturvedi, N., R. Klein, J. Christensen, J. Ahmed, and A. Kojic (2010) "Algorithms for Advanced Battery-Management Systems," *Control Systems Magazine, IEEE*, **30**(3), pp. 49–68.

[15] Di Domenico, D., A. Stefanopoulou, and G. Fiengo (2008) "Reduced order lithium-ion battery electrochemical model and extended kalman filter state of charge estimation," *ASME Journal of Dynamic Systems, Measurement and Control-Special Issue on Physical System Modeling*.

[16] Klein, R., N. Chaturvedi, J. Christensen, J. Ahmed, R. Findeisen, and A. Kojic (2010) "State estimation of a reduced electrochemical model of a lithium-ion battery," in *American Control Conference (ACC), 2010*, IEEE, pp. 6618–6623.

[17] Speltino, C., D. Di Domenico, G. Fiengo, and A. Stefanopoulou (2009) "Experimental identification and validation of an electrochemical model of a Lithium-Ion Battery," in *Proceedings of 2009 IEEE European Control Conference*.

[18] Santhanagopalan, S. and R. White (2006) "Online estimation of the state of charge of a lithium ion cell," *Journal of power sources*, **161**(2), pp. 1346–1355.

[19] Doyle, M., T. Fuller, and J. Newman (1993) "Modeling of galvanostatic charge and discharge of the lithium/polymer/insertion cell," *Journal of the Electrochemical Society*, **140**, p. 1526.

[20] Smith, K., C. Rahn, and C. Wang (2007) "Control oriented 1D electrochemical model of lithium ion battery," *Energy conversion and management*, **48**(9), pp. 2565–2578.

[21] Speltino, C., D. Di Domenico, G. Fiengo, and A. Stefanopoulou (2009) "Comparison of reduced order lithium-ion battery models for control applications," in *Decision and Control, 2009 held jointly with the 2009 28th Chinese Control Conference. CDC/CCC 2009. Proceedings of the 48th IEEE Conference on*, IEEE, pp. 3276–3281.

[22] Vetter, J., P. Novak, M. Wagner, C. Veit, K. Möller, J. Besenhard, M. Winter, M. Wohlfahrt-Mehrens, C. Vogler, and A. Hammouche (2005) "Ageing mechanisms in lithium-ion batteries," *Journal of power sources*, **147**(1), pp. 269–281.

[23] ARORA, P., R. WHITE, and M. DOYLE (1998) "Capacity fade mechanisms and side reactions in lithium-ion batteries," *Journal of the Electrochemical Society*, **145**(10), pp. 3647–3667.

[24] Hatzell, K., A. Sharma, and H. Fathy (2012) "A Survey of Long-Term Health Modeling, Estimation, and Control of Lithium-Ion Batteries : Challenges and Opportunities," in *American Control Conference (ACC), 2012*.

[25] Ramadass, P., B. Haran, R. White, and B. Popov (2003) "Mathematical modeling of the capacity fade of Li-ion cells," *Journal of power sources*, **123**(2), pp. 230–240.

[26] Rong, P. and M. Pedram (2006) "An analytical model for predicting the remaining battery capacity of lithium-ion batteries," *Very Large Scale Integration (VLSI) Systems, IEEE Transactions on*, **14**(5), pp. 441–451.

[27] Peterson, S., J. Apt, and J. Whitacre (2010) "Lithium-ion battery cell degradation resulting from realistic vehicle and vehicle-to-grid utilization," *Journal of Power Sources*, **195**(8), pp. 2385–2392.

[28] Saha, B., K. Goebel, S. Poll, and J. Christophersen (2009) "Prognostics methods for battery health monitoring using a Bayesian framework," *Instrumentation and Measurement, IEEE Transactions on*, **58**(2), pp. 291–296.

[29] Wang, J., P. Liu, J. Hicks-Garner, E. Sherman, S. Soukiazian, M. Verbrugge, H. Tataria, J. Musser, and P. Finamore (2011) "Cycle-life model for graphite-LiFePO4 cells," *Journal of Power Sources*, **196**(8), pp. 3942–3948.

[30] Santhanagopalan, S., Q. Guo, P. Ramadass, and R. White (2006) "Review of models for predicting the cycling performance of lithium ion batteries," *Journal of power sources*, **156**(2), pp. 620–628.

[31] Chiang, Y., W. Sean, and J. Ke (2011) "Online estimation of internal resistance and open-circuit voltage of lithium-ion batteries in electric vehicles," *Journal of Power Sources*.

[32] Pop, V., H. Bergveld, P. Notten, J. Op het Veld, and P. Regtien (2009) "Accuracy analysis of the State-of-Charge and remaining run-time determination for lithium-ion batteries," *Measurement*, **42**(8), pp. 1131–1138.

[33] Tang, X., X. Mao, J. Lin, and B. Koch (2011) "Capacity estimation for Li-ion batteries," in *American Control Conference (ACC), 2011*, IEEE, pp. 947–952.

[34] Verbrugge, M. (2007) "Adaptive, multi-parameter battery state estimator with optimized time-weighting factors," *Journal of applied electrochemistry*, **37**(5), pp. 605–616.

[35] Lee, S., J. Kim, J. Lee, and B. Cho (2008) "State-of-charge and capacity estimation of lithium-ion battery using a new open-circuit voltage versus state-of-charge," *Journal of power sources*, **185**(2), pp. 1367–1373.

[36] Lee, J., O. Nam, and B. Cho (2007) "Li-ion battery SOC estimation method based on the reduced order extended Kalman filtering," *Journal of Power Sources*, **174**(1), pp. 9–15.

[37] Ning, G., R. White, and B. Popov (2006) "A generalized cycle life model of rechargeable Li-ion batteries," *Electrochimica acta*, **51**(10), pp. 2012–2022.

[38] Astrom, K. and B. Wittenmark (1994) *Adaptive control*, Addison-Wesley Longman Publishing Co., Inc.

[39] Sorenson, H. (1970) "Least-squares estimation: from Gauss to Kalman," *Spectrum, IEEE*, **7**(7), pp. 63–68.

[40] Green, M. and J. Moore (1986) "Persistence of excitation in linear systems," *Systems & control letters*, **7**(5), pp. 351–360.

[41] McWhorter, T. and L. Scharf (1993) "Cramer-Rao bounds for deterministic modal analysis," *Signal Processing, IEEE Transactions on*, **41**(5), pp. 1847–1866.